

# **Investigating The Application of Channel Boundary Conditions for Model Calibration and Validation**

Hwai-Ping (Pearce) Cheng<sup>1</sup>, Earl V. Edris<sup>2</sup>, David R. Richards<sup>3</sup>

<sup>1</sup>Coastal and Hydraulics Laboratory, US Army Engineer Research and Development Center, 3909 Halls Ferry Road, Vicksburg, MS 39180-6199; PH (601) 634-3699; FAX (601) 634-4208; email: [hwai-ping.cheng@erdc.usace.army.mil](mailto:hwai-ping.cheng@erdc.usace.army.mil)

<sup>2</sup>Coastal and Hydraulics Laboratory, US Army Engineer Research and Development Center, 3909 Halls Ferry Road, Vicksburg, MS 39180-6199; PH (601) 634-3378; FAX (601) 634-4208; email: [earl.v.edris@erdc.usace.army.mil](mailto:earl.v.edris@erdc.usace.army.mil)

<sup>3</sup>Information Technology Laboratory, US Army Engineer Research and Development Center, 3909 Halls Ferry Road, Vicksburg, MS 39180-6199; PH (601) 634-2126; FAX (601) 634-4208; email: [david.r.richards@erdc.usace.army.mil](mailto:david.r.richards@erdc.usace.army.mil)

## ***Abstract***

This study investigated how the stage-type and the flow-type boundary conditions may impact the channel flow solutions in order to address issues concerning adequate channel boundary conditions for model calibration and validation. It is revealed that using the stage-type boundary condition and using the flow-type boundary condition yield the same results as long as the conditions are consistent. Because flow may be more sensitive to the change of system input (e.g., boundary condition, source/sink, model parameter, etc.) than stage (or depth), it is suggested that the more accurate measured stage data be used for calibration with the less accurate measured flow data employed as a secondary check point to ensure correct calibration-validation outcomes. A sensitivity analysis to determine an adequate time-step size for the desired computational mesh is essential for valid model calibration and validation.

## ***Introduction***

Should flux-type or stage-type boundary conditions be used in calibrating a channel routing model or is one type better than the other? Some people have argued that the flux-type boundary condition is definitely better than the stage-type boundary condition because the application of the stage-type boundary condition could result in a vast supply (inflow) or withdrawal (discharge) of water to maintain the prescribed stage on the desired boundary, and that mass conservation will only be maintained with the application of the measured flow. However, it is usually more troublesome and expensive to measure adequate channel flow than water stage in the field, and the measured flow in a channel routing system is generally much less accurate than the

measured stage (<http://ga.water.usgs.gov/edu/measureflow.html>). A critical question to be answered is, "Is it suitable to use the more accurate field stage data to set up boundary conditions without introducing artificial boundary flow in model calibration?" The main goal of this study is to address this boundary condition issue both theoretically and numerically.

### *A Conceptual Model of Channel Flow*

As depicted in Figure 1(a), a channel reach is discretized with three elements (cells) and four nodes, where Element 1 has Nodes 1 and 2 as its element nodes, Element 2 Nodes 2 and 3, and Element 3 Nodes 3 and 4. For each element, water may be introduced into (source) or removed from (sink) the channel reach through rainfall (i.e., R1, R2, and R3), evapotranspiration (i.e., ET1, ET2, and ET3), infiltration/seepage (i.e., I1, I2, and I3), man-induced injection and withdrawal (i.e., S1, S2, and S3), and the flow processes due to energy gradients (i.e., Q1, Q2, Q3, and Q4). For the case of incompressible flow, the mass conservation equation of each element can be written as follows.

$$\frac{dV}{dt} = \sum_i Source_i - \sum_j Sink_j \quad (1)$$

where  $V$  = the water volume of the element of interest [ $L^3$ ];  $t$  = time [ $t$ ];  $Source_i$  = the  $i$ -th source term for the element [ $L^3/t$ ]; and  $Sink_j$  = the  $j$ -th sink term for the element [ $L^3/t$ ].

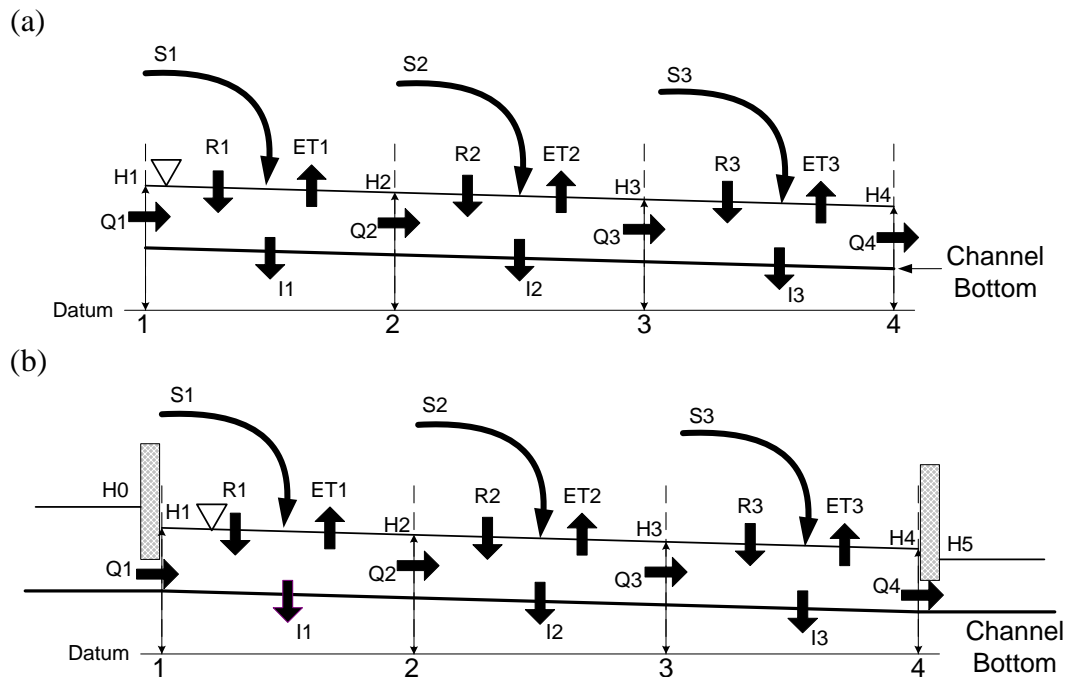


**Figure 1. A conceptual channel flow model: (a) no gate-controlled structures; (b) gate-controlled structures included**

Based on Eq. (1), the mass conservation equations of the three elements in Figure 1 are

$$\frac{dV_1}{dt} = (Q1 + R1 + S1) - (Q2 + ET1 + I1) \quad (2)$$

$$\frac{dV_2}{dt} = (Q2 + R2 + S2) - (Q3 + ET2 + I2) \quad (3)$$

$$\frac{dV_3}{dt} = (Q3 + R3 + S3) - (Q4 + ET3 + I3) \quad (4)$$

It is noted that the water volume of an element can be represented by the water stages of its two end nodes (e.g., H1 and H2 for Element 1) provided channel cross-sectional geometry, the water stage at a specific location is closely related to all the source and sink terms nearby (e.g., H2 increases with R1 and R2 but decreases with I1 and I2), and the flow at a specific location is determined based on the energy slope that depends on the stage variation around the location. Therefore, water stage and flow are two variables that not only depend on each other but also work together to satisfy mass conservation locally and globally. In other words, water stage and flow are closely inter-related and determined by all the physical processes involved. In fact, water stage and flow are uniquely determined by the conditions of the system (e.g., boundary conditions and sources/sinks) as well as the physical processes involved in the system. The law of mass conservation and the flow dynamics observed in channel hydrology and hydraulics have been used to construct mathematical models to compute stage and flow both analytically and numerically in the past decades (Chow, 1959; Jain, 2001). Such uniqueness allows us to expect identical results from solving the channel routing equations with either the stage-type or the flow-type boundary conditions in model calibration and validation as long as they are consistent, i.e., accounting for the same set of physical processes and corresponding to the same system condition. For example, to compute water stage and flow in Figure 1, two different simulation set-ups can be made: one has Q1 and Q4 given as the flux-type boundary conditions to compute Q2, Q3, and H1 through H4; the other has H1 and H4 given as the stage-type boundary conditions to compute H2, H3, and Q1 through Q4. If there is no numerical error, using the computed H1 and H4 from the first simulation as the boundary conditions in the second simulation will generate identical results, and vice versa.

To highlight the significance of including needed physical processes, the three-element channel reach is bounded by two gate structures in Figure 1(b). Suppose both gate structures are controlled by the desired operational rules, the channel inflow, i.e., Q1, and discharge, i.e., Q4, are then determined not only by energy gradient but also by the operational rules and the associated rating curves. If the measured stage is taken as the boundary condition without taking into account the operational rules, the physical process of gate operation is missing in the model and the result would likely deviate from actual observations as a result of different operations. That is, when the

measured H1 and H4 are used to set up the stage-type boundary condition without considering gate operation, the computed Q1 and Q4 will not match the measured Q1 and Q4 because the model does not include the gate operations that play a role in the determination of boundary flow. In other words, the model using stage-type boundary conditions without accounting for appropriate gate operations is inconsistent with the model using flow-type boundary conditions that incorporate gate operations.

Theoretically, the measured stage and/or the measured flow can be employed as the boundary conditions in model calibration and validation, and the computational results should be identical if there are no measurement errors or numerical errors and consistency between heads, flows, and operating rules are maintained. In practice, however, there are always errors from both field measurements and numerical computations in model calibration and validation work. The following sections provide details using the WASH123D numerical code and a 1-D channel routing test example to further investigate the applications of the two types of boundary conditions.

### *Numerical Experiments*

**WASH123D.** The WASH123D finite element numerical code is a first-principle, physics-based modeling tool that conceptualizes a watershed system as a combination of 1-D channel networks, 2-D overland regimes, and 3-D subsurface media [Yeh et al., 2006]. The physical model parameters to be calibrated and validated are the Manning's roughness coefficients for 1-D channel flow (i.e.,  $n_1$ ), the Manning's roughness coefficients for 2-D overland flow (i.e.,  $n_2$ ), and saturated hydraulic conductivities for 3-D subsurface flow (i.e.,  $K$ ) given fixed soil curves. Each element can be assigned a different material type to account for heterogeneity, and each material may have its own set of physical model parameters given supporting field data. The capability of computing 1-D channel routing by solving the 1-D X-section-averaged diffusion wave equations was employed in this study. The semi-Lagrangian numerical method is used to solve the 1-D diffusion wave equation [Lin et al., 2004].

**Test Example.** A hypothetical 1-D channel network system (Figure 2) was constructed for the numerical experiments conducted in this study. The network system contained three inlets (i.e., channel inflow, Nodes 1, 15, and 43), one outlet (i.e., channel discharge, Node 42), one dead end (i.e., Node 68), three channel junctions (i.e., JT-1, JT-2, and JT-3), and seven reaches (i.e., R-1 through R-7). Each channel reach was specified with a cross-sectional geometry with the cross-sectional area increasing from upstream down (Table 1). A seven-day simulation was conducted for each run. Hourly rainfall and hourly evapotranspiration profiles were applied to the entire network (Figure 3). An initial stage condition was assumed and the initial flow velocities were computed in WASH123D based on a diffusive wave equation. The Manning's roughness coefficient was set to 0.03 for every channel element. Table 2 lists test cases employed.

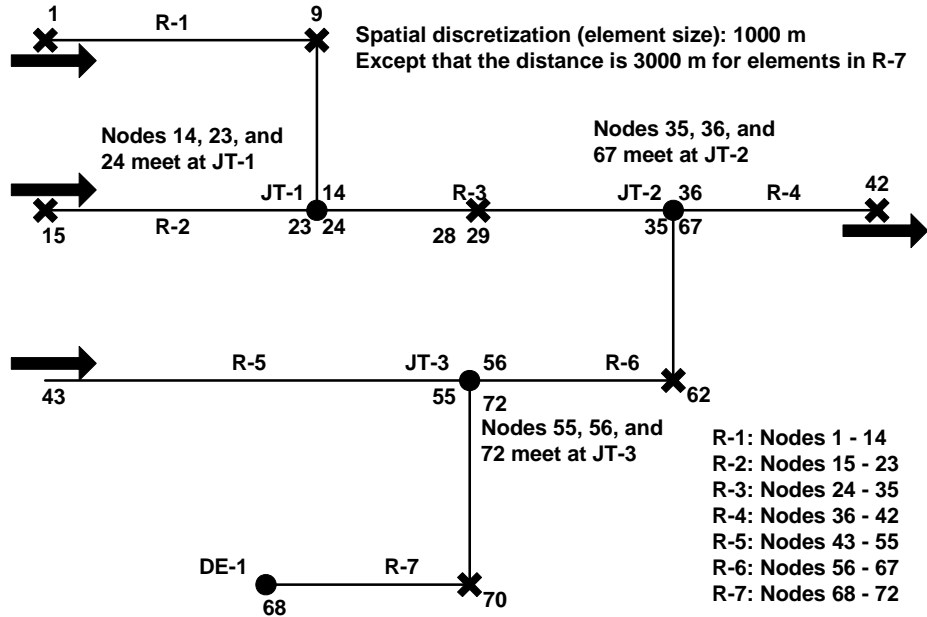


Figure 2. Channel network of the test example: locations marked with crosses are where the computed stages and flows are compared between different cases

Table 1. Cross-section geometries of the seven reaches

Reach ID	X-section geometry	Reach ID	X-section geometry
R-1		R-5 & R-7	
R-6		R-2	
R-3		R-4	

**Table 2. Test cases**

Case ID	Case Description
1	Stage boundary conditions only, $\Delta t = 10$ seconds (Base Case)
2	Use the flow solution from Case 1 to prepare hourly flow boundary conditions for Nodes 1, 15, and 43 (i.e., the upstream boundary nodes)
3	Use the flow solution from Case 1 to prepare 15-minute flow boundary conditions for Nodes 1, 15, and 43 (i.e., the upstream boundary nodes)
4	Same as Case 1 except that $\Delta t = 30$ seconds
5	Same as Case 1 except that $\Delta t = 60$ seconds
6	Same as Case 1 except that a rating-curve (i.e., depth-dependent flow) boundary condition is applied to Node 42 (i.e., the downstream boundary node)
7	Use the stage solution from Case 6 to prepare 15-minute stage boundary condition for Node 42 (i.e., the downstream boundary node)
8	Same as Case 7 except that the flow solution from Case 6 is used to prepare hourly flow boundary conditions for Nodes 1, 15, and 43 (i.e., the upstream boundary nodes)

**Hourly Rainfall & ET**

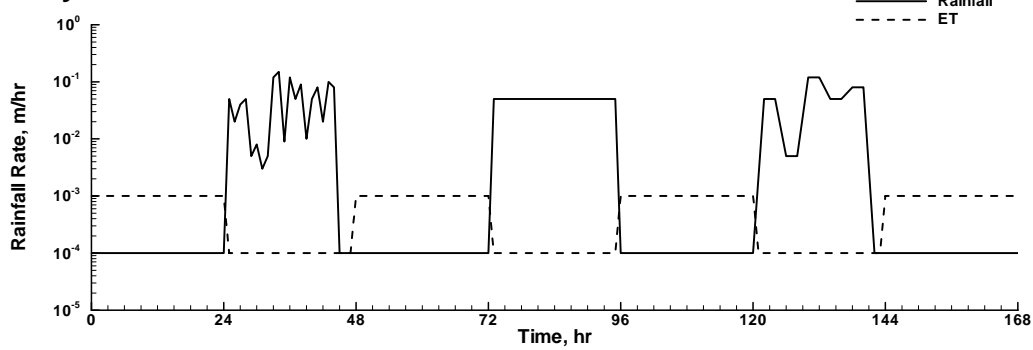
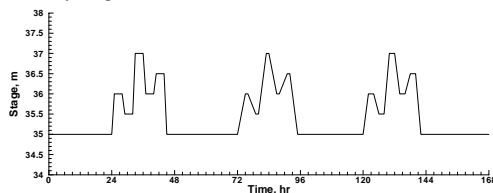
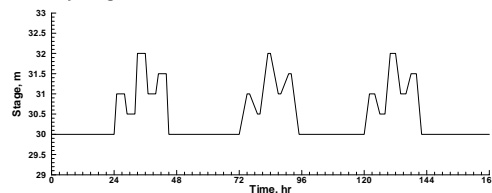


**Figure 3. Hourly Rainfall and ET profiles**

**Boundary Stage of Nodes 1 & 43**



**Boundary Stage of Node 15**



**Boundary Stage of Node 42**

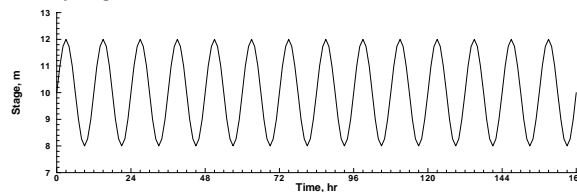


**Figure 4. Stage boundary conditions for Case 1**

For the base condition (i.e., Case 1), hourly stage boundary conditions (Figure 4) were applied to both the three inlets and the one outlet. The stage and flow solutions were output every 15 minutes for analysis and used in the development of related boundary conditions for other associated testing runs and conditions.

Both Cases 2 and 3 used the flow solution obtained from Case 1 to set up upstream flow-type boundary conditions at the three inlets, where the hourly flow profile was employed in Case 2, and the 15-minute flow profile was used in Case 3. Both Cases 4 and 5 were the same as Case 1 except different time step sizes (i.e.,  $\Delta t$ ) were considered for computation. Case 6 differed from Case 1 in the downstream boundary condition, where a rating-curve boundary condition was employed at Node 42. The stage solution from Case 6 at Node 42 was then used in Case 7 to set up the downstream boundary condition. The flow solution from Case 7 at the three inlets was later employed in Case 8 to set up the upstream boundary condition.

**Results & Discussion.** Table 2 lists the values for the two types of deviation measures, *Average Mean Absolute Deviation (AMAD)* and *Average Root Mean Square Deviation (ARMSD)* [Kneale et al., 2001; Montgomery and Runger, 1999] for case comparisons: Cases 1 and 6 were the reference groups considered for the first four and the last two comparisons, respectively. These two deviations are defined as

$$AMAD = \frac{\sum_{it=1}^{n_t} \left( \frac{\sum_{i=1}^n |C_{it,i} - O_{it,i}|}{n} \right)}{n_t} \quad (5)$$

$$ARMSD = \frac{\sum_{it=1}^{n_t} \left( \sqrt{\frac{\sum_{i=1}^n |C_{it,i} - O_{it,i}|^2}{n}} \right)}{n_t} \quad (6)$$

where  $n$  = number of comparisons between the values from the reference and the comparative groups, both are computed here, within each time step;  $n_t$  = number of time steps included for data comparison;  $C_{it,i}$  = the  $i$ -th value for comparison from the comparative group that is associated with the  $it$ -th time step;  $R_{it,i}$  = the  $i$ -th value for comparison from the reference group the is associated with the  $it$ -th time step. Basically, the two groups of data are in close agreement when *AMAD* and *ARMSD* are small.

**Table 3. Overall deviation measures**

Case Comparison	Depth Deviation Measures			
	<i>AMAD (m)</i>	<i>AMAD %<sup>+</sup></i>	<i>ARMSD (m)</i>	<i>ARMSD %<sup>+</sup></i>
Case 1 vs. Case 2	0.0057	0.09	0.0070	0.11
Case 1 vs. Case 3	0.0018	0.03	0.0024	0.04
Case 1 vs. Case 4	0.0030	0.05	0.0037	0.06
Case 1 vs. Case 5	0.0657	1.02	0.1037	1.61
Case 6 vs. Case 7	0.0014	0.02	0.0034	0.05
Case 6 vs. Case 8	0.0057	0.09	0.0070	0.11
Case Comparison	Flow Deviation Measures			
	<i>AMAD (m<sup>3</sup>/hr)</i>	<i>AMAD %<sup>^</sup></i>	<i>ARMSD (m<sup>3</sup>/hr)</i>	<i>ARMSD %<sup>^</sup></i>
Case 1 vs. Case 2	2,414	0.14	3,152	0.19
Case 1 vs. Case 3	847	0.05	1,203	0.07
Case 1 vs. Case 4	1,675	0.10	2,808	0.17
Case 1 vs. Case 5	44,238	2.63	120,216	7.16
Case 6 vs. Case 7	1,078	0.06	4,580	0.27
Case 6 vs. Case 8	2,404	0.14	3,149	0.19

<sup>+</sup> The deviation percentage is the *AMAD* or the *ARMSD* of depth divided by the average channel water depth throughout the entire simulation period that was about 6.45 m

<sup>^</sup> The deviation percentage is the *AMAD* or the *ARMSD* of flow divided by the average channel flow throughout the entire simulation period that was about  $1.68 \times 10^6$  m<sup>3</sup>/hr

The deviation percentages associated with *AMAD* and *ARMSD* were estimated based on the average channel water depth and flow throughout the entire simulation period. Eqs. (7) and (8) were used to calculate the deviation percentage for stage and flow, respectively.

$$\text{Depth Deviation \%} = \frac{\text{AMAD (or ARMSD)}}{\text{Average Water Depth}} \times 100\% \quad (7)$$

$$\text{Flow Deviation \%} = \frac{\text{AMAD (or ARMSD)}}{\text{Average Flow}} \times 100\% \quad (8)$$

For example, the average water depth over the entire channel network during the 7-day simulation period is about 6.45 m, and the *AMAD* and the *ARMSD* are 0.0057 m and 0.0070 m, respectively, in the comparison between Case 1 and Case 2. Thus, the corresponding deviation percentages (i.e., 0.09% and 0.11%) are calculated with Eqs. (7) and (8). Table 3 shows higher deviation percentages in flow comparison than those in depth comparison, suggesting that flow is more sensitive than depth (or stage) in our test cases.

Figures 5 and 6 compare the computed water stage and flow, respectively, at seven selected locations between Cases 1 and 2, while Figures 7 and 8 compare Cases 6 and 8. The seven locations include two inlets (i.e., Nodes 1 and 15), the only outlet (i.e., Node 42), mid-point locations in Reaches R-1 (i.e., Node 9), R-3 (i.e., Node 29), R-6 (i.e., Node 62), and R-7 (i.e., Node 70), as marked with crosses in Figure 2.

**Case 1 vs. Case 2**

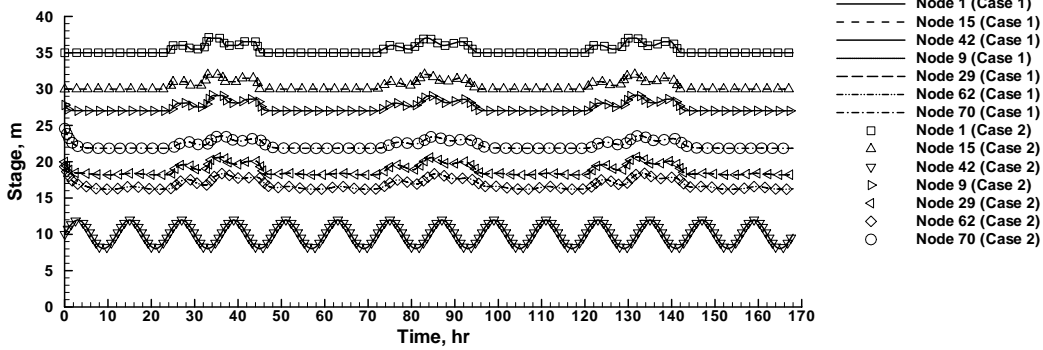


**Figure 5. Comparison of the computed stage at 7 locations as specified in Figure 2 between Case 1 (with hourly stage BC's) and Case 2 (with calculated hourly inflow BC's)**

**Case 1 vs. Case 2**

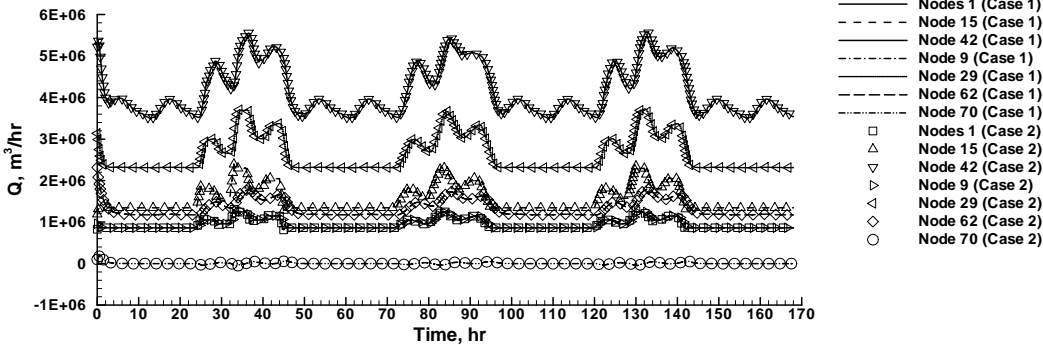


**Figure 6. Comparison of the computed flow 7 locations as specified in Figure 2 between Case 1 (with hourly stage BC's) and Case 2 (with calculated hourly inflow BC's)**

**Case 6 vs. Case 8**

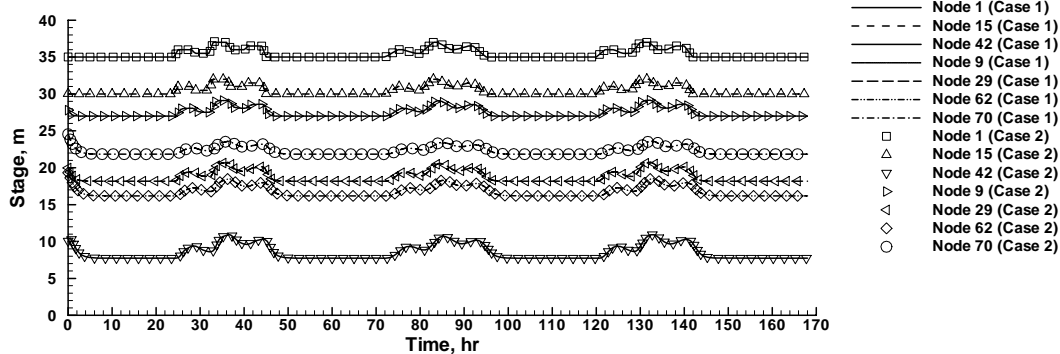


**Figure 7. Comparison of the computed stage at 7 locations as specified in Figure 2 between Case 6 (same as 1 except for rating curve outflow BC) and Case 8 (same as 6 with calculated flow from 7 used as upstream inflow BC)**

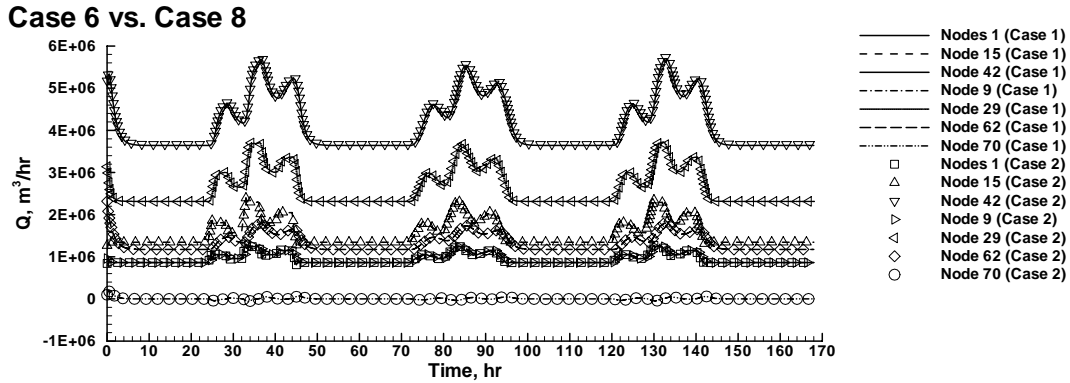


**Figure 8. Comparison of the computed flow at 7 locations as specified in Figure 2 between Case 6 (same as 1 except for rating curve outflow BC) and Case 8 (same as 6 with calculated flow from 7 used as upstream inflow BC)**

All the deviation measures listed in Table 3 except for the comparison between Case 1 and case 5 show excellent agreement for the compared pairs (depth *AMAD* % < 0.1 %, depth *ARMSD* % < 0.12 %, flow *AMAD* % < 0.15 %, flow *ARMSD* % < 0.28 %), indicating that as long as consistent boundary conditions are used, it does not matter whether they are of stage type (e.g., Case 1), flow type (e.g., Case 8), or mixed type (e.g., Cases 2, 3, 6, and 7). Figures 5 through 8 also support this statement. When 15-minute flow boundary conditions (Case 3) were used, the results had a better agreement to those of Case 1 in both stage and flow when compared to the results of Case 2 in which hourly flow boundary conditions were used (i.e., smaller error measure values for the comparison between Cases 1 and 3 than between Cases 1 and 2, Table 2). This demonstrates that a higher data resolution for boundary condition profiles introduce less deviation errors in the computational results. It also implies that the accuracy of a validated model depends upon the resolution of measured data used for model calibration and validation.

In Figures 9 through 12, the stage and flow comparisons are plotted at the outlet (i.e., Node 42), mid-point location in Reach R-3 (i.e., Node 29), and mid-point location in Reach R-6 (i.e., Node 62), as marked with crosses in Figure 2. Differences in stage and flow at these three nodes are not obvious in Figures 9 and 10, indicating limited impacts from the increased time-step size (from 10 seconds in Case 1 to 30 seconds in Case 4) at those locations. The differences become apparent in Figures 11 and 12, demonstrating the impact of time-step size in numerical simulation at these locations. It is noted that great flow deviations occur at Node 29 (i.e., the outlet) in Figure 12 even though a periodic stage boundary condition was applied to that node (Figure 11). This emphasizes the need to conduct sensitivity analyses to determine an adequate time-step size for accurate computations. The deviation measures provided in Table 3 for the comparisons between Cases 1 and 4 and between Cases 1 and 5 also indicate increasing differences with time step size (the stage *AMAD* increases from 0.0030 to 0.0657 m, and the flow *AMAD* increases from 1,657 to 44,238 m<sup>3</sup>/hr when the time step size increases from 30 seconds in Case 4 to 60 seconds in Case 5).

It is noteworthy that the stage and flow differences between Cases 1 and 5 are minimal at another 4 locations marked with crosses in Figure 2 (i.e., Nodes 1, 9, 15, and 70) even through the time step size has been increased to 60 seconds. This suggests that the impact of time-step size at a more upstream location is smaller than at a downstream location due to error propagation in computation.

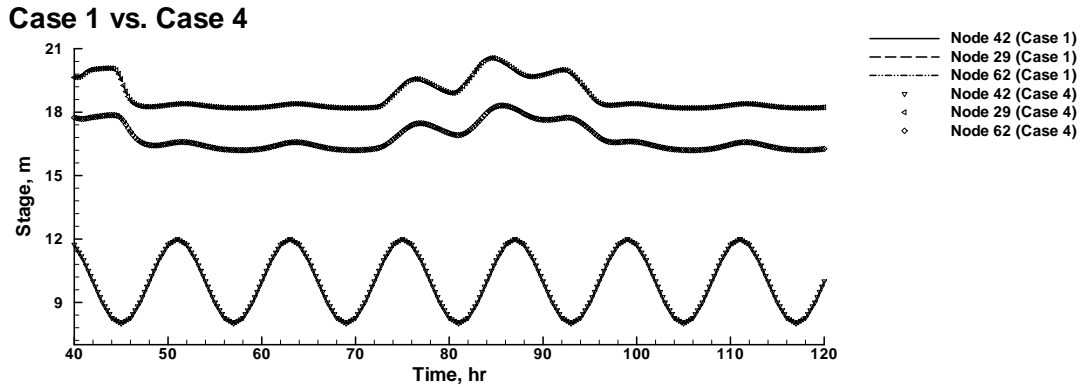


Figure 9. Comparison of the computed stage 3 locations as specified in Figure 2 between Case 1 ( $\Delta t = 10$  seconds) and Case 4 ( $\Delta t = 30$  seconds)

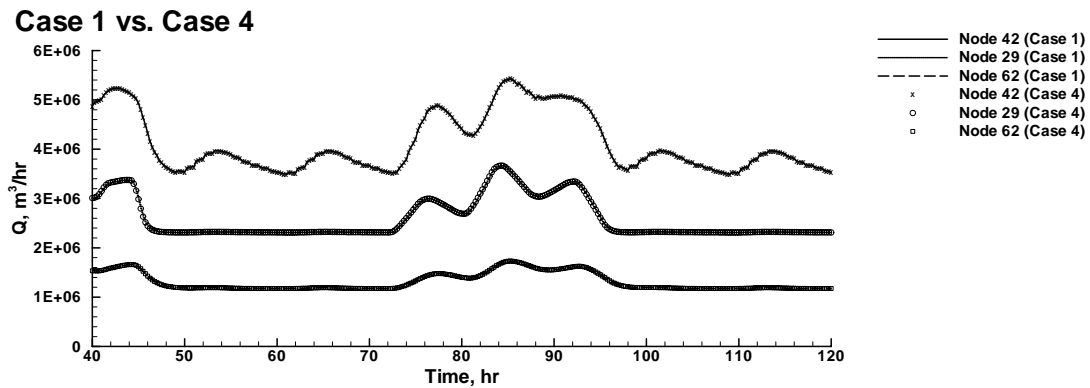


Figure 10. Comparison of the computed flow at 3 locations as specified in Figure 2 between Case 1 ( $\Delta t = 10$  seconds) and Case 4 ( $\Delta t = 30$  seconds)

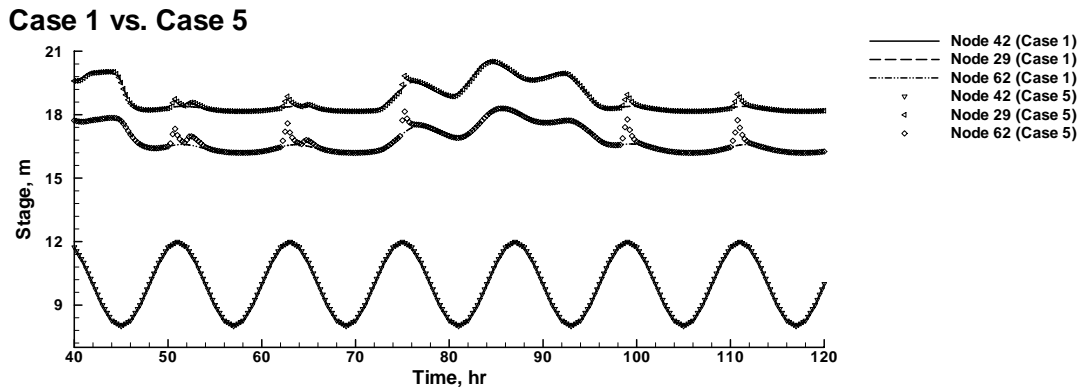


Figure 11. Comparison of the computed stage at 3 locations as specified in Figure 2 between Case 1 ( $\Delta t = 10$  seconds) and Case 5 ( $\Delta t = 60$  seconds)

### Case 1 vs. Case 5

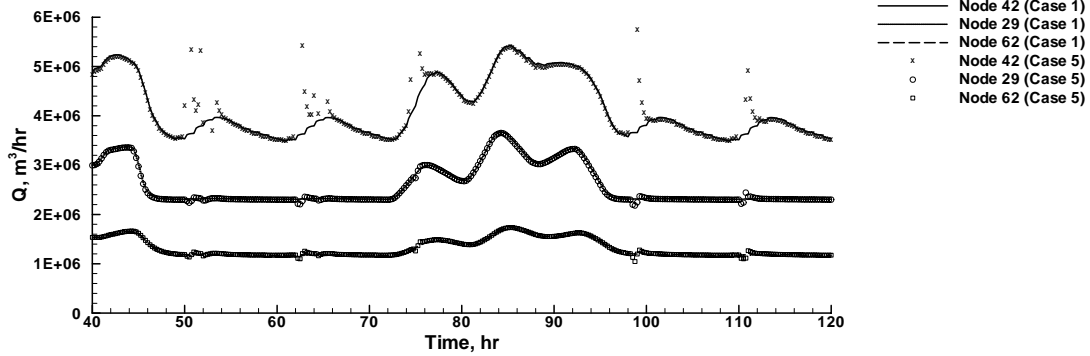


Figure 12. Comparison of the computed flow at 3 locations as specified in Figure 2 between Case 1 ( $\Delta t = 10$  seconds) and Case 5 ( $\Delta t = 60$  seconds)

### Case 1 vs. Case 5

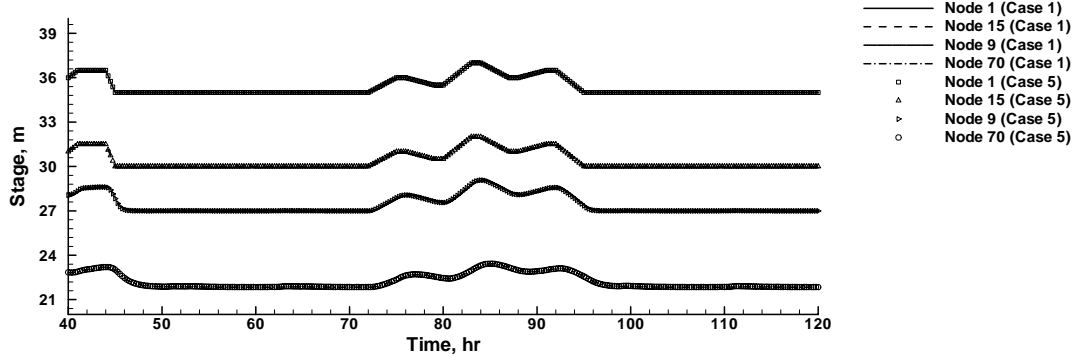


Figure 13. Comparison of the computed stage at another 4 locations as specified in Figure 2 between Case 1 ( $\Delta t = 10$  seconds) and Case 5 ( $\Delta t = 60$  seconds)

### Case 1 vs. Case 5

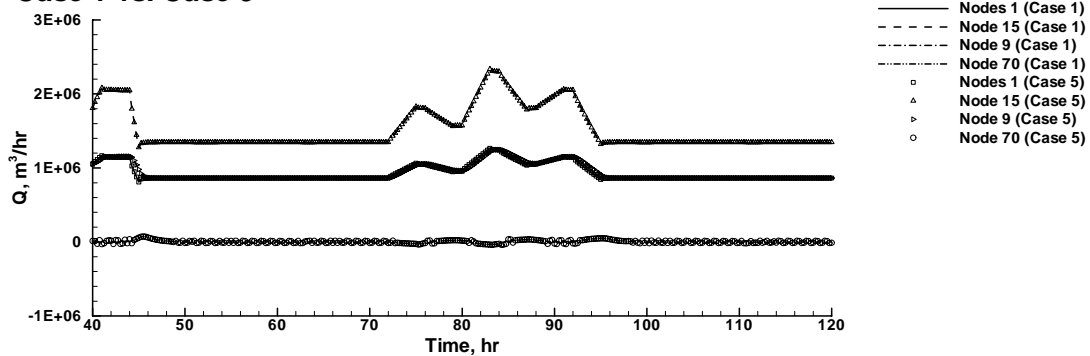


Figure 14. Comparison of the computed flow at another 4 locations as specified in Figure 2 between Case 1 ( $\Delta t = 10$  seconds) and Case 5 ( $\Delta t = 60$  seconds)

## **CONCLUSIONS**

A three-element conceptual model of channel flow was employed to demonstrate how closely the flow-type and the stage-type boundary conditions are related to each other. The necessity of taking into needed physical processes and using consistent boundary conditions to generate correct solutions for the simulated system was also discussed. A test example was constructed in this study to further examine how the stage-type and the flow-type boundary conditions may impact the channel flow solutions in model calibration and validation through numerical experiments. It included eight cases concerning a channel network. Stage-type boundary conditions and flow-type boundary conditions were found to yield the same results as long as they are consistent (i.e., see comparisons between Cases 1 and 2, Cases 1 and 3, Cases 6 and 7, and Cases 6 and 8). Because flow may be more sensitive than depth (or stage), it is suggest that the more accurate measured stage data be used for calibration with the less accurate measured flow data employed as a secondary check point to ensure correct calibration-validation outcomes.

It is also noted that time-step size plays a crucial role in numerical computation (see comparison between Cases 1 and 4 and Cases 1 and 5). A sensitivity analysis to determine an adequate time-step size for a given computational mesh is a MUST in model calibration and validation. In general, smaller time-step sizes are needed for meshes of higher spatial resolution.

## **Acknowledgments**

This study was supported by the System-Wide Water Resources Program (SWWRP) of US Army Engineer Research and Development Center (ERDC). Permission was granted by the Chief of Engineer to publish this information.

## **References**

Chow, V. T., 1959, *Open-Channel Hydraulics*, 680 pp, McGraw-Hill.

Jain, S. C., 2001, *Open-Channel Flow*, 328 pp, John-Wiley & Sons.

Kneale, P.E., L. See, and A. Smith, 2001, *Towards Defining Evaluation Measures for Neural Network Forecasting Models*, In: *Proceedings of GeoComputation*, Brisbane, 24-26 Sep 2001.

Lin, H.-C., H.-P. Cheng, E. V. Edris, and G.-T. Yeh, 2004, *Modeling Surface and Subsurface Hydrologic Interactions in a South Florida Watershed near the Biscayne Bay*, *Computational Methods in Water Resources XV*, June 13-17, 2004, CMWR CD-ROM (Volume II, II.7.8 Lin\_174), The University of North Carolina at Chapel Hill, North Carolina, USA.

Montgomery, D. C. and G. C. Runger, 1999, *Applied Statistics and Probability for Engineers*, 2nd ed., 815 pp, John Wiley & Sons.

Yeh, G.-T., G. Huang, H.-P. Cheng, F. Zhang, H.-C. Lin, E. Edris, and D. Richards, 2006, *A First-Principle, Physics-Based Watershed Model: WASH123D*, Chapter 9, *Watershed Models*, 653 pp., Edited by V. P. Singh and D. K. Frevert, CRC Press, Taylor & Francis Group.